

Conformers and Photochemistry of Propyl Nitrites: A Matrix Isolation Study

Edit Mátyus, Gábor Magyarfalvi, and György Tarczay*

Laboratory of Molecular Spectroscopy, Institute of Chemistry, Eötvös University, P.O. Box 32, H-1518, Budapest 112, Hungary

Received: September 21, 2006; In Final Form: October 27, 2006

The infrared spectra of both constitutional isomers (*n* and *i*) of propyl nitrite have been recorded in an Ar matrix. Conformational analysis and assignments of the vibrational transitions have been carried out on the basis of quantum chemical calculations. Assignment of spectral lines to different conformers was also aided experimentally, by utilizing the different rate of photodecomposition of the conformers, as well as by employing conformational cooling using a supersonic jet as the inlet source for matrix deposition. The rate of photodecomposition is primarily determined by the steric alignment of the nitrite group, whereas jet cooling affects mainly the conformation of the alkyl tail. On the basis of these experimental observations and computational predictions two to three conformers of isopropyl nitrite and eight conformers of *n*-propyl nitrite were identified. After broadband ultraviolet–visible (UV–vis) photolysis of isopropyl nitrite in the matrix, HNO, acetone, HNO·acetone complex, acetaldehyde, and nitrosomethane were identified as the main products. Furthermore, in a small amount, NO and possibly the isopropoxy radical were also present in the matrix. Photolysis of *n*-propyl nitrite yielded HNO, propanal, and their 1:1 complex as the main products together with a small amount of NO and *cis*-1-nitrosopropanol.

1. Introduction

Because alkyl nitrites are well-known sources of alkoxy radicals, which are important intermediates of combustion and atmospheric chemical processes,¹ their photochemistry has been studied extensively during the past few decades. In the case of larger alkyl nitrites, the photochemical pathways can depend on the conformers of the precursor. Consequently, the distribution of the products including their conformational ratios can depend on the conformational population of the precursor alkyl nitrites themselves. Hence, to fully understand the photochemical processes, one has to analyze the conformational distribution of the precursors first.

One of the experimental methods best suited for conformational analysis is matrix-isolation infrared (MI-IR) spectroscopy. The basic assumption in most matrix-isolation investigations is that the vapor-phase conformational population is maintained in the low-temperature (6–10 K) matrix. This assumption is usually fulfilled if the barrier of the interconversion between the different conformers is larger than a few kJ/mol. Even when the matrix is annealed at 35 K, only conformers with barriers not higher than ca. 10–12 kJ/mol can interconvert.²

Attribution of spectral transitions to different conformers can be aided by the comparison of spectra of matrices deposited from various temperatures. In such experiments not only conformational labeling is carried out but also the relative enthalpies or Gibbs energies of different conformers can be estimated.³ The applicability of this method can be limited if the sample is thermally unstable, like alkyl nitrites, whereas simple cooling is not efficient because of the condensation of the sample onto the wall of either the inlet source or the sample reservoir. For these compounds alternative methods have to be found, for example, supersonic jet cooling or the exploitation of different photosensitivities of the different conformers.

Besides the cooling of the rotational and the vibrational degrees of freedom, adiabatic expansion by a supersonic jet can

also result in depletion of the higher energy conformers of multiconformer molecules, helping the conformational analysis. In spite of this advantage, matrix deposition using a supersonic jet inlet source is not a widespread experimental technique. The first attempt to couple matrix isolation experiments with supersonic jet cooling was made by Felder and Günthard in 1979 and 1982.^{4,5} In their experiment the expanding sample was diluted before the deposition by a crossed argon beam entering through an effusive inlet source. The conformational cooling was not very effective, which was explained later by the fact that the effusive argon beam likely messed up the conformational cooling achieved by the expansion.³ Almost 20 years later, Vidya et al.² in 1996 and Kudoh et al.³ in 1998 constructed a more successful jet-matrix isolation setup, expanding a diluted mixture of the sample and argon directly into the vacuum chamber.^{2,3,6–13}

It is important to note that the sample after the supersonic expansion is not in a thermodynamic equilibrium.¹⁴ First of all, the cooling is not equally effective for the different translational, rotational, and vibrational degrees of freedom. Second, the conformer distribution cannot be simply given by the Boltzmann equation. High-energy conformers can only be efficiently depopulated if at least one of the barriers of interconversion to lower-energy conformers is low enough. It is generally found that high-energy conformers separated from the other minima of the potential energy surface (PES) by barriers higher than ca. 10–15 kJ/mol cannot be depopulated easily under the usual supersonic expansion conditions.^{2,15}

As mentioned above, the other phenomenon that could be utilized to aid the conformational labeling of the alkyl nitrite vibrational transitions is the different photosensitivity of the conformers. Photolysis of methyl nitrite in cryogenic matrices was already studied at the dawn of matrix isolation by Brown and Pimentel,¹⁶ Jacox et al.,^{17,18} and Huber et al.^{19–21} These studies were followed by the matrix photolysis experiments on ethyl nitrite,²² *tert*-butyl nitrite,²³ and several cycloalkyl nitrites.²⁴

The general conclusion of these studies was that the rate of decomposition considerably depends on the wavelength of the irradiating ultraviolet–visible (UV–vis) light and on the steric alignment of the CONO moiety (i.e., anti or syn). Furthermore, it was generally assumed that the first step of the photoinduced chemical processes is identical to the process observed in the gas phase independently of the alkyl tail; i.e., it is a homolytic bond cleavage resulting in alkoxy and NO radicals. Nevertheless, direct evidence for the presence of the alkoxy radical in a cryogenic matrix was only found when laser-induced fluorescence detection was used for the investigation of the photodecomposition products of CH₃ONO.²⁵ Alkoxy radicals have not yet been identified in the infrared spectra of photolyzed matrix isolated alkyl nitrites. This is mainly due to the fact that alkoxy radicals can recombine or can go through further reactions with NO formed in the same matrix cage. These reactions and the final reaction products depend on the experimental conditions and on the alkyl chain.

In the case of methyl nitrite, the two possible orientations of the ONO moiety with respect to the alkyl chain results in two conformers, anti and syn. The conformer ratio was observed to be ca. 35% anti and 65% syn when the sample was deposited from room temperature.^{26,27} At the beginning of irradiation with $\lambda_{\text{exc}} > 345$ nm UV–vis light, a growth of the infrared bands belonging to anti-CH₃ONO was observed at the expense of the bands of the syn conformer.¹⁸ In contrast to this, irradiation of the matrix sample with $\lambda_{\text{exc}} = 390$ nm UV light has completely cleared off the anti conformer from beside the syn conformer.²⁶ Upon broadband photolysis the main products were H₂CO, HNO, and their hydrogen-bonded 1:1 complex. Photolysis of this complex produced either the anti (using $\lambda_{\text{exc}} = 345$ nm radiation) or the syn (using $\lambda_{\text{exc}} \geq 645$ nm radiation) conformer of CH₂(OH)(NO).^{20,21} After prolonged broadband photolysis of matrix isolated methyl nitrite (or nitromethane), the dominant products were CO, NO, HNCO, and H₂CO·HNO.¹⁷

Ethyl nitrite has one torsional degree of freedom more than methyl nitrite, so more conformers come to the scene. According to microwave spectroscopic studies²⁸ the relative abundances are 34% anti–gauche, 16% syn–gauche, and 50% syn–trans at room temperature. Irradiation at 365 nm, the wavelength of the S₁(nπ*) ← S₀(nπ) excitation, produced CH₃CHO, HNO and their hydrogen-bonded 1:1 complex. An important result of this study was that in the photolysis of CD₃CH₂ONO, the CD₃CHO·HNO complex was formed exclusively; i.e., the nitroxyl hydrogen came exclusively from the C_α atom. The next step in the photolysis was the formation of syn-nitrosoethanol.²²

Of the two possible conformers of *tert*-butyl nitrite only the anti conformer was present in a significant amount in an Ar matrix when the gas mixture was deposited from room temperature.²³ As a result of broadband UV–vis irradiation *syn-tert*-butyl nitrite had appeared, and acetone and nitrosomethane were produced. The isomerization was dominant if the concentration of the nitrite was higher in the matrix, whereas in dilute matrices the decomposition became more important.

UV irradiation (365 nm) of matrix isolated cyclobutyl nitrite caused a ring opening reaction producing 4-nitrosobutanal as the main product. In the case of cyclopentyl nitrite the complex of cyclopentanone and HNO was formed besides the analogous ring-opening product, 5-nitrosopentanal. The irradiation of cyclohexyl, cycloheptyl and cyclooctyl nitrites resulted mainly in the production of the corresponding cycloalkyl ketones complexed with HNO.²⁴

The aim of the present work is to identify the different conformers and the photolysis products of matrix isolated

n-propyl and isopropyl nitrites by Fourier-transform infrared spectroscopy (FT–IR). We show that besides quantum chemical calculations, conformational cooling by supersonic jet expansion and exploiting the different photodecomposition rates of the different conformers can help in the assignment of the conformers. Following the assignment of the conformers of propyl nitrites, the photodecomposition products and the possible photochemical reaction paths followed upon UV–vis irradiation are analyzed. We also intended to go one step further than earlier matrix isolation studies on alkyl nitrites and look for signs of the species formed in the first step of the photolysis, i.e., the alkoxy radical and nitrogen monoxide.

2. Experimental Details

Propyl nitrite samples were prepared according to the literature.²⁹ The purity of the samples was checked by recording the IR spectrum of the neat liquid and the vaporized samples. The degassed samples were mixed with argon (from Messer, purity 99.996%) in a 1:1500–1:2000 mole ratio in a glass (for the effusive sample inlet) or a stainless steel (for the supersonic jet inlet) vacuum line.

The gas mixture was deposited onto a CsI window mounted on a Janis CCS-350R cold head cooled by a CTI Cryogenics 22 closed-cycle refrigerator unit. The temperature of the copper cold head was controlled by a Lake Shore 321 thermostat equipped with a silicon diode thermometer. During the deposition of the matrix mixture, UV–vis irradiation and FT–IR measurements, the temperature was kept in the range 8–10 K. For annealing the temperature was increased to 30–35 K and was kept there for 5–10 min.

Deposition of the gas mixture was carried out in two different ways. In one set of experiments a simple effusive inlet was used. In these experiments the stagnation pressure was 1–0.8 bar and the flow rate was ca. 2–4 mmol/h. In the other set of experiments a pulsed supersonic jet (General Valve, orifice of 200 μm diameter) was used for deposition. The jet was mounted perpendicularly to the CsI window, the distance between the outlet of the jet and the window was ca. 5 cm. The stagnation pressure in the jet experiments was 1–2 bar. The opening time of the jet pulses was 300–400 μs, the repetition rate was set to 4–6 or 6–9 Hz, which resulted in a ca. 1–2 mmol/h flow rate.

In the photolysis experiments the matrix was irradiated by a Cathodeon HPK 125 W high-pressure mercury lamp (the most intense lines are at ca. 580, 578, 548, 440, 405, 365, and 310 nm) through a quartz window mounted on the vacuum chamber.

Infrared spectra were recorded by a Bruker IFS 55 Fourier-transform infrared (FT–IR) spectrometer equipped with a KBr beamsplitter and a DTGS detector. A total of 250 (or 500) scans were accumulated at 1 cm⁻¹ (or 0.5 cm⁻¹) resolution. Blackman–Harris three-term (or boxcar) apodization function, Mertz phase correction using phase resolution of 32 cm⁻¹, and zero filling factor of 4 (or 2) were applied.

3. Computational Details

Geometry optimization of the possible conformers of *n*-propyl and isopropyl nitrites was carried out at the B3LYP/6-31G*^{30,31} level of theory. These optimized geometries were used as input for G2³² calculations to obtain Gibbs energies, from which the Boltzmann distribution of the different conformers was predicted at the temperature of the effusive inlet source (room temperature, 298 K). Barrier heights between two conformers were estimated by the difference of the (not zero-point-corrected) B3LYP/6-31G* electronic energy of the optimized saddle point and one of the appropriate equilibrium structures. All the above-

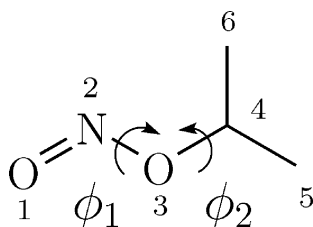


Figure 1. Labeling scheme of isopropyl nitrite. Hydrogen atoms are labeled as follows: C(4)H(7), C(5)H(8)H(9)H(10), C(6)H(11)H(12)H(13). ϕ_1 : O(1)N(2)O(3)C(4) \angle , ϕ_2 : N(2)O(3)C(4)H(7) \angle .

TABLE 1: Relative Gibbs Energies (kJ mol⁻¹) and Abundances of the Different Conformers of Isopropyl Nitrite

conformer	$(\phi_1, \phi_2)^a$	$\Delta_r G^\ominus(0 \text{ K})^b$	$\Delta_r G^\ominus(298 \text{ K})^b$	% abundance ^c
AT	(180, 180)	8.1 [5.9]	10.5 [3.7]	10
AC	(180, 0)	0.0 [0.0]	0.0 [0.0]	42
ST	(0, 180)	14.9 [17.3]	19.1 [15.9]	0
SC+(SC-)	(1, 35)	0.1 [2.9]	3.6 [1.4]	48

^a Torsional angles in degrees (see Figure 1) as obtained at the B3LYP/6-31G* level of theory. ^b Calculated at the B3LYP/6-31G* and the [G2] level of theory. ^c Calculated from $\Delta_r G^\ominus(\text{G2})$ at 298 K.

mentioned calculations were performed by the Gaussian 03 program package.³³

Vibrational frequencies and infrared intensities were calculated at the B3LYP/6-31G* level of theory using the scaled quantum mechanical (SQM) force field^{34,35} method with scale factors determined by Baker et al.³⁵ These vibrational frequency calculations including the total energy distribution (TED)³⁶ of normal modes between the different internal coordinates were performed by the Parallel Quantum Solutions (PQS) 3.2 program package.³⁷

4. Results and Discussion

4.1. Theoretical Results. *4.1.1. Isopropyl Nitrite.* There are two different internal rotations in isopropyl nitrite that connect the different conformers to each other. These are the rotations along the ONOC and NOCH torsional angles denoted as ϕ_1 and ϕ_2 , respectively (see Figure 1). Geometry optimizations starting from all possible structures with $\phi_1 = 0, 180^\circ$ and $\phi_2 = 0, 180^\circ$ resulted in four minima on the PES at the B3LYP/6-31G* level of theory.

These are the anti-cis (AC), the anti-trans (AT), the syn-cis (SC), and the syn-trans (ST) conformers, where the labels refer to the ϕ_1 and ϕ_2 torsional angles, respectively. Because the SC conformer exists in two optically active forms, SC- and SC+, this conformer has to be considered with a statistical weight of 2 as compared to the other conformers for calculation of relative abundances. (The nonpolarized light used in our experiments does not distinguish between enantiomers; therefore, these species are equivalent under our experimental setup, resulting in this statistical factor.)

Computed Boltzmann distributions, based on the computed G2 Gibbs energies at 298 K, predict that three conformers, AT, AC, and SC, are expected to have considerable population in the vapor phase (see Table 1). The most abundant conformer is SC with nearly the same ratio, 48%, as the second one, AC, 42%. The relative abundance of the AT conformer is small, about 10%.

In addition to the relative abundances of conformers, estimates of the barrier heights between conformers are also required for the analysis of supersonic jet deposition experiments. It is shown in Table 2 that the conformers of isopropyl nitrite are separated by high (> 50 kJ/mol) energy barriers except for the intercon-

TABLE 2: Relative Energies (kJ mol⁻¹) of Transition States of Isopropyl Nitrite

transition state ^a	ΔE^b vs minimum _I	ΔE^b vs minimum _{II}
(A/S)+T+ (85, 176)	55.6 AT (180, 180)	49.6 ST (0, 180)
(A/S)-G+ (-90, 52)	56.8 AC (180, 0)	57.7 SC+ (1, 35)
SSt+ (0, 119)	36.6 SC+ (1, 35)	22.0 ST (0, 180)
ASt+ (180, 119)	13.3 AC (180, 0)	5.5 AT (180, 180)

^a (ϕ_1, ϕ_2) : torsional angles in degrees (see Figure 1). (A/S) refers to an angle in between the anti and syn orientations, i.e., torsional angle around 90° . ^b ΔE : relative energy of the transition state compared to the respective minima, calculated at the B3LYP/6-31G* level of theory.

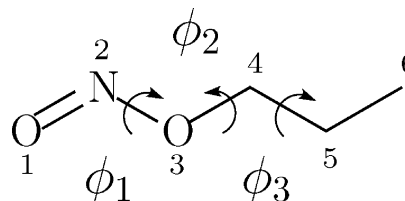


Figure 2. Labeling scheme of *n*-propyl nitrite. Hydrogen atoms are labeled as follows: C(4)H(7)H(8), C(5)H(9)H(10), C(6)H(11)H(12)H(13). ϕ_1 : O(1)N(2)O(3)C(4) \angle , ϕ_2 : N(2)O(3)C(4)C(5) \angle , ϕ_3 : O(3)C(4)C(5)C(6) \angle .

version of SC- \rightarrow ST and AC- \rightarrow AT, which are internal rotations along the NOCH torsion. Along these two coordinates the conformational cooling in supersonic expansion can be efficient. Of these paths the SC- \rightarrow ST is irrelevant in light of the nearly zero relative abundance of the ST conformer. Cooling along the AC- \rightarrow AT coordinate might have a slight effect on the spectra; i.e., the ratio of the more stable AC conformer can increase. The very low, ~ 5 kJ/mol, AT \rightarrow ASt+ barrier indicates that depopulation of the AT conformer can happen not only during the supersonic expansion but also during the trapping of sample on the cold window. This means that the conformer ratios, observable in the matrix, can depend on the actual conditions of deposition, e.g., temperature, deposition rate or scattering angle, and momentum of the colliding molecules at the cold window. However, as the relative amount of the AT conformer is small, these effects are not expected to strongly alter the infrared spectra.

4.1.2. n-Propyl Nitrite. Conformational search on the PES of *n*-propyl nitrite was performed along the ϕ_1 (ONOC), ϕ_2 (NOCC), and ϕ_3 (OCCC) torsional angles (see Figure 2). Starting geometry optimizations using the B3LYP/6-31G* level of theory from each combination of $\phi_1 = 0, 180^\circ$, $\phi_2 = 0, \pm 60, \pm 120, 180^\circ$, and $\phi_3 = \pm 60, 180^\circ$ resulted in eight minima.

Of these minimum structures three are syn ($\phi_1 \approx 0^\circ$) and five are anti ($\phi_2 \approx 180^\circ$) conformers (see Table 3 for details). These conformers are denoted as ASt-G+, A+St-G+, A+St-G-, ST+G-, STT, SG-T-, SG-G-, and ASt-G+, where the letters stand for the steric alignment (syn or anti) around the ONOC torsion, the second one (staggered, gauche, or trans) belongs to the NOCC torsion, and the third one labels (gauche or trans) the OCCC torsional angle. The + and - signs after the letters refer to the sign of the torsional angle. All of the conformers, except STT, have mirror image pairs. According to the results of G2 calculations all of these conformers are present in considerable concentration in the gas phase at 298 K (see Table 3).

The calculated relative energies of the interconversion barriers between conformers are listed in Table 4. In the case of *n*-propyl nitrite the situation is more complex than was found for isopropyl. On the basis of the heights of the barriers one can sort the calculated transition structures roughly into three groups.

TABLE 3: Relative Gibbs Energies (kJ mol⁻¹) and Abundances of the Different Conformers of *n*-Propyl Nitrite

conformer	(ϕ_1, ϕ_2, ϕ_3) ^a	$\Delta_r G^\ominus$ (0 K) ^b	$\Delta_r G^\ominus$ (298 K) ^b	% abundance ^c
ASt-G+ (ASt+G-)	(180, -117, 65)	3.23 [0.00]	2.11 [0.00]	43
A+St-T- (A-St+T+)	(178, -106, -176)	3.06 [1.06]	1.24 [2.21]	18
A+St-G- (A-St+G+)	(178, -107, -60)	3.34 [1.24]	1.90 [2.46]	16
ST+G- (ST-G+)	(0, 179, -64)	0.00 [1.11]	0.27 [3.79]	9
STT	(0, 180, 180)	0.07 [1.40]	0.00 [3.87]	4
SG-T- (SG+T+)	(0, -87, -176)	2.34 [3.03]	3.02 [5.66]	4
SG-G- (SG+G+)	(0, -87, -59)	2.68 [3.53]	3.55 [6.29]	3
SSt-G+ (SSt+G-)	(0, -108, 65)	4.49 [4.72]	4.00 [7.02]	3

^a Torsional angles in degrees (see Figure 2) as obtained at the B3LYP/6-31G* level. ^b Calculated at the B3LYP/6-31G* and the [G2] levels of theory, respectively. ^c Abundance: calculated from $\Delta_r G^\ominus$ (G2).

TABLE 4: Relative Energies (kJ mol⁻¹) of Transition States of *n*-Propyl Nitrite

transition state ^a		ΔE vs minimum ^{a,b}		ΔE vs minimum ^{a,b}			
AT-G-	(180, -177, -63)	4.5	A+St-G-	(178, -107, -60)	4.6	ASt+G-	(180, 117, -65)
A+St-St-	(179, -113, -116)	13.8	A+St-G-	(178, -107, -60)	13.9	A+St-T-	(178, -106, -176)
A+St-St+	(179, -111, 123)	13.9	A+St-G-	(178, -107, -60)	14.0	A+St-T-	(178, -106, -176)
AC+G-	(180, 15, -79)	18.9	A+St-G-	(178, -107, -60)	19.0	ASt+G-	(180, 117, -65)
S-St-T-	(-2, -125, -177)	4.9	STT	(0, -180, -180)	3.0	SG-T-	(0, -87, -176)
STG-	(0, 180, -120)	13.2	STT	(0, 180, 180)	13.5	ST+G-	(0, 179, -64)
S-St-G-	(-2, -125, -61)	5.2	ST+G-	(0, 179, -64)	2.8	SG-G-	(0, -87, -59)
S-St-G+	(-1, -121, 66)	4.8	ST+G-	(0, 179, -64)	0.2	SSt-G+	(0, -108, 65)
S+G-St-	(1, -81, -114)	12.3	SG-T-	(0, -87, -176)	12.0	SG-G-	(0, -87, -59)
S+G-St+	(1, -85, 118)	13.1	SG-T-	(0, -87, -176)	10.6	SSt-G+	(0, -108, 65)
S+G-C+	(2, -90, 7)	17.0	SG-G-	(0, -87, -59)	14.8	SSt-G+	(0, -108, 65)
S+C+G-	(1, 9, -82)	41.1	SG-G-	(0, -87, -59)	38.9	SSt+G-	(0, 108, -65)
S-C-G+	(-2, -10, 83)	38.9	SSt-G+	(0, -108, 65)	41.1	SG+G+	(0, 87, 59)
(S/A)-G-T-	(-91, -73, -176)	59.2	SG-T-	(0, -87, -176)	57.5	A+St-T-	(178, -106, -176)
(S/A)-G-G-	(-91, -73, -58)	58.2	SG-G-	(0, -87, -59)	56.7	A+St-G-	(178, -107, -60)
(S/A)-G-G+	(-93, -84, 69)	58.4	SSt-G+	(0, -108, 65)	59.2	ASt-G+	(180, -117, 65)
(S/A)+G-T-	(84, -87, -176)	60.1	SG-T-	(0, -87, -176)	58.4	A+St-T-	(178, -106, -176)
(S/A)+G-G-	(82, -90, -61)	59.3	SG-G-	(0, -87, -59)	57.8	A+St-G-	(178, -107, -60)
(S/A)+G-G+	(-, -, -)	-	SSt-G+	(0, -108, 65)	-	ASt-G+	(180, -117, 65)
(S/A)+T+G-	(86, 174, -64)	56.6	SG-G-	(0, -87, -59)	55.1	A+St-G-	(178, -107, -60)
(S/A)+T+G+	(87, 178, 63)	54.5	SSt-G+	(0, -108, 65)	55.4	ASt-G+	(180, -117, 65)

^a (ϕ_1, ϕ_2, ϕ_3): torsional angles in degrees (see Figure 2). (A/S) refers to an angle in between the anti and syn orientations, i.e., torsional angle around 90°. ^b ΔE : relative energy of the different transition states compared to the respective minima calculated at the B3LYP/6-31G* level of theory. ^c Calculations did not converge to yield saddle points between these conformers.

Interconversion along ϕ_1 (ONOC) torsion as an approximate reaction coordinate has a typically high, >50 kJ/mol, energy barrier. Thus efficient conformational cooling; i.e., syn-anti conversion is not expected in our jet experiments. Along the ϕ_3 (OCCC) coordinate the energy barriers are moderately high, typically in the range 10–20 kJ/mol. For this coordinate supersonic jet cooling might be observable. The transition structures belonging to the third group connect the conformers along the ϕ_2 (NOCC) coordinate. These structures are located only a few kJ/mol above the minima. Not only can a barrier of this height be efficiently overcome by supersonic cooling, but also the energy of collision of molecules with the cold surface can be high enough for conformational transformations along these shallow paths. These include the interconversion of A+St-G- \rightleftharpoons ASt+G-, STT \rightleftharpoons SG-T-, and SG-G- \rightleftharpoons ST+G- \rightleftharpoons SSt-G+.

4.2. Experimental Results. 4.2.1. Conformational Analysis.

4.2.1.a. Isopropyl Nitrite. On the basis of theoretical calculations, three conformers, AT, AC, and SC, are expected to be present in the matrix deposited from room temperature.

It has already been discussed that the barrier height between the two predominant conformers is high, whereas the low-energy barriers connect only conformers with low abundance to these conformers. In good agreement with this prediction the spectra obtained using supersonic jet and effusive matrix deposition are not significantly different. Hence, this technique cannot help the conformational analysis in this case.

Upon broadband UV-vis irradiation two groups of peaks were found in the IR spectra that decreased with a significantly different rate (see Figure 3). Theoretical calculations clearly show that the frequency of the N=O stretching fundamental of anti conformers is higher by approximately 50 cm⁻¹ than that of syn conformers. Accordingly, the peaks at 1653 and 1605 cm⁻¹ belong to the N=O stretching excitation of the anti and the (SC) syn conformers, respectively. Because the intensity of the peak at 1653 cm⁻¹ was decreasing faster upon irradiation than the intensity of the other peak, it can be concluded that the anti conformers had decomposed faster than the syn (SC) conformer under our experimental conditions. On the basis of this observation, the peaks of the infrared spectra can easily be sorted out to the syn (SC) and the anti conformers. To demonstrate this, the infrared spectra recorded before and after UV-vis irradiation were subtracted from each other using an appropriate factor to eliminate the peaks of anti or syn conformers. These are shown as spectra b and c in Figure 3, where (b) shows the negative peaks of the syn (SC) conformer and the products, and in (c) the positive peaks correspond to the products and the negative peaks to the AC and AT anti conformers.

On the basis of theoretical calculations and photochemical results, the most intense peaks centered at 1605, 1109, 931, 924, 755 and 692 cm⁻¹ can be assigned to the SC, and peaks at 1653, 1182, 1148, 1134, 962, 890, 878, 783 and 604 cm⁻¹ to the AC

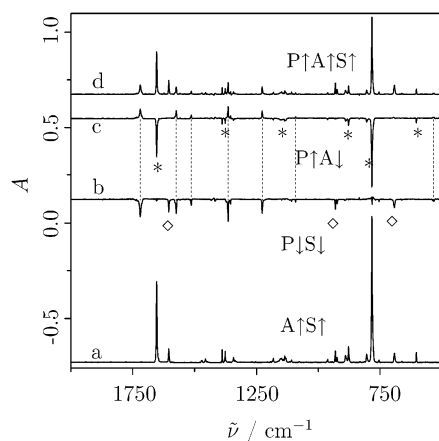


Figure 3. Infrared spectra measured with a resolution of 1 cm^{-1} before and after a short period of photolysis of isopropyl nitrite. (a) Isopropyl nitrite in argon matrix before photolysis (A_0). (b) $A_0 - 1.9A_{\text{photo}}$ (contains the negative peaks of the SC conformer and the products). (c) $A_{\text{photo}} - A_0$ (positive peaks belong to the products; the negative peaks to the AC and AT conformers). (d) After 10 min of photolysis (A_{photo}). Photoproduct (P) peaks are connected with a dashed line. Key: (*) anti (A); (◇) syn (S) conformers.

conformer. A summary assignment of the spectrum is shown in Table 5; for further details, see the Supporting Information.

From these assignments it can be generally concluded that the computed and experimental vibrational frequencies are in good agreement, except for the modes that have significant contribution from the internal coordinates corresponding to the ONO functional group. As an example, the N(2)O(1) stretching fundamental of the {AC/SC} conformer is observed at $\{1653/1605\}\text{ cm}^{-1}$, whereas it is predicted by calculations to be $\{1684/1628\}\text{ cm}^{-1}$. Similarly, the peaks corresponding to the N(2)O(3) stretching mode of the AC conformer and the O(1)N(2)O(3) bending mode of the SC conformer, observed at 783 and 692 cm^{-1} , respectively, are 15–20 cm^{-1} overestimated by the calculations.

Most of the other vibrational modes are predicted more accurately by the SQM B3LYP calculation, usually they agree within 10 cm^{-1} with the experimental results, facilitating the spectral assignment. One of the remaining discrepancies between the calculations and the experimental results is the appearance

of two close-lying peaks in the spectrum at 890 and 878 cm^{-1} . In this region only one transition is expected by the calculations, a vibrational transition of the AC conformer at 874 cm^{-1} . A likely explanation of this discrepancy is the doubling of this peak in the spectrum due to matrix site effects.

Identification of the AT conformer is less certain than that of the two more abundant conformers. First, its presence cannot be ascertained by the N(2)O(1) stretching fundamental, because it likely overlaps with the corresponding transition of the AC conformer. The identification of the AT conformer can mostly be based on two small intensity peaks at 1131 and 832 cm^{-1} , and on a more intense peak at 804 cm^{-1} . The position of the small peaks are in line with the calculations, but the assignment of the peak at 804 cm^{-1} is somewhat unambiguous. The main reason is the calculations predict the vibrational frequency of AC to be about 20 cm^{-1} higher (798 cm^{-1}) than that of the AT conformer (777 cm^{-1}), whereas the AC conformer is assigned to a band lower in frequency by about 20 cm^{-1} than the observed spectral band, which was assigned to the AT conformer. Our choice in favor of this assignment was based on the following arguments.

First, the two bands in question certainly originate from isopropyl nitrite, because these bands cannot be assigned to complexes with water or other possible impurities. Second, photosensitivity studies show that both peaks correspond to species with anti sterical alignment of the CONO group, whereas the close-lying band at 755 cm^{-1} corresponds to a syn form. If both of these two bands are assigned to anti forms, then the remaining question is whether the two bands are originated from the same conformer or not.

It is unlikely that both bands belong to the AT conformer, because AC is predicted to be more abundant; consequently, its most intense peak is expected to show up in this spectral region. On the basis of experiments, it cannot be ruled out that both peaks correspond to the AC conformer. In this case the appearance of these two vibrational features could be explained by splitting due to matrix site effects. This would mean that the most intense peak, and as a consequence none of the spectral transitions of the AT conformer, could not be identified in the experimental spectrum.

If we accept at least qualitatively the conformer ratios predicted for the temperature of deposition, then a vibrational

TABLE 5: Abridged Assignment of the MI-IR Spectrum of Isopropyl Nitrite

$\tilde{\nu}_{\text{obs}}$	I_{obs}^a	Ph ^b	conf. ^c	$\tilde{\nu}_{\text{calc}}^d$	I_{calc}^d	TED ^e
1653	vs	anti	AT	1684	206	94% stre N2O1
			AC	1694	238	94% stre N2O1
1605	s	syn	SC	1628	157	95% stre N2O1
1182	m	anti	AC	1190	16	15% bend H13C6C4, 15% bend H10C5C4
1134	m	anti	AC	1129	10	23% stre C4C6, 23% stre C4C5
1131	w	anti	AT	1133	12	24% stre C4C6, 24% stre C4C5
1109	m	syn	SC	1119	26	21% bend H9C3C4
962	m		AC	958	12	27% stre C4O3, 35% bend O1N2O3
931	m	syn	SC	946	148	49% bend O1N2O3
			SC	935	18	12% stre C4C2, 18% bend H12C2C4, 10% bend H13C2C4, 14% bend H9C3C4
924	m	syn	SC	921	5	16% bend H11C2C4, 10% bend H13C2C4, 18% bend H8C3C4
878	m	anti	AC	874	157	24% stre C4C6, 24% stre C4C5, 11% bend O1N2O3
832	w		AT	843	137	28% stre C4C6, 28% stre C4C5, 17% bend O1N2O3
804	w	anti	AT	777	226	10% stre C4C6, 10% stre C4C5, 28% stre C4O3, 34% stre O3N2
783	vs	anti	AC	798	368	10% stre C4C6, 10% stre C4C5, 29% stre C4O3, 45% stre O3N2
755	m	syn	SC	756	68	22% stre C4O3, 33% stre O3N2
692	m	syn	SC	712	110	36% stre C4O3, 34% stre O3N2, 13% bend O1N2O3
604	m	anti	AC	599	16	10% stre C4O3, 24% stre O3N2, 31% bend O1N2O3

^a $\tilde{\nu}_{\text{obs}}$: measured frequency in cm^{-1} , I_{obs} : measured intensity (w, weak; m, medium; s, strong; vs, very strong). ^b Ph.: assignment by the different photodecomposition rates. ^c Conf.: conformer (AC, AT, SC). ^d Obtained at the SQM B3LYP/6-31G* level of theory ($\tilde{\nu}_{\text{calc}}$ in cm^{-1} , I_{calc} in km/mol units). ^e TED: total energy distribution of normal modes (components with a ratio higher than 10%) over internal coordinates (stre, stretching; bend, bending; tors, torsional coordinate). Labels are in agreement with Figure 1.

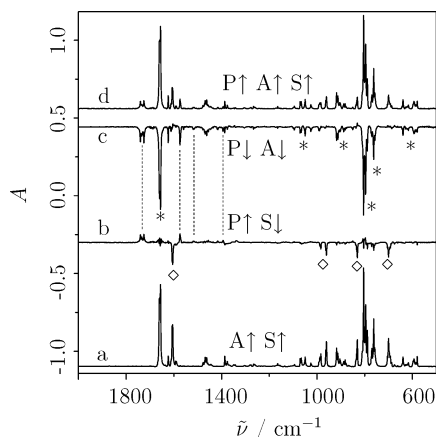


Figure 4. Infrared spectra measured with a resolution of 1 cm^{-1} before and after a short period of photolysis of *n*-propyl nitrite. (a) *n*-Propyl nitrite in argon matrix before photolysis (A_0). (b) $A_{\text{photo}} - A_0$ (positive peaks belong to the products; the negative peaks to the syn type conformers). (c) $A_0 - 2A_{\text{photo}}$ (contains the negative peaks of the anti type conformers and the products). (d) After 45 min of photolysis (A_{photo}). Photoproduct (P) peaks are connected with a dashed line. Key: (*) anti (A); (◇) syn (S) conformers.

transition of both conformers should appear in this spectral region. Because AC is predicted to be much more abundant, and its calculated infrared intensity is larger, the stronger band at 783 cm^{-1} has to be assigned to the AC conformer, and the other band at 804 cm^{-1} to the AT conformer.

4.2.1.b. *n*-Propyl Nitrite. As discussed before, theoretical calculations predict that all eight conformers of *n*-propyl nitrite are present in a considerable amount at room temperature in the vapor phase.

Upon UV–vis irradiation, two groups of peaks could be distinguished. The intensity of peaks belonging to the first group decreased rapidly, but the peaks in the other group were almost unaltered during a short period of photolysis. This behavior implies the existence of two groups of conformers that have significantly different photochemical sensitivity. Chemical intuition suggests that the orientation of the ONOC functional group is likely to have the most important effect on the reactivity, hence these two groups should correspond to the anti and syn type conformers. On the basis of theoretical calculations, the N=O vibrational fundamental of the anti conformers is undoubtedly higher in energy, by ca. 70 cm^{-1} , than the corresponding fundamental of the syn forms. Based on the observation that, in the frequency region where the N=O stretching vibrational fundamental is expected, the intensity of peaks between 1656 and 1661 cm^{-1} did not change upon irradiation, but the intensity of peaks around 1605 cm^{-1} decreased quickly (see Figure 4), it can be concluded that under our experimental conditions the syn conformers decomposed faster than the anti forms. This is in contrast with the observation for isopropyl nitrite where the decomposition of the anti conformers was faster. Because the absorption cross section and hence the rate of decomposition depends on the overlap of the spectral lines of the irradiating light and the $S_1 \leftarrow S_0$ transition of the alkyl nitrite, this difference can likely be explained by the difference in the $S_1 \leftarrow S_0$ excitation energy of the isopropyl nitrite and *n*-propyl nitrite species.

To help the assignments, the syn or the anti peaks can be eliminated from the spectrum by subtracting the appropriately weighted spectra measured before and after the photolysis from each other (see spectra b or c in Figure 4).

The individual syn conformers can hardly be differentiated on the basis of photochemical experiments. This is for several

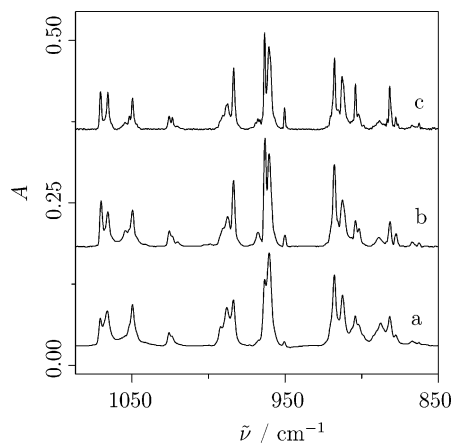


Figure 5. Infrared spectra of *n*-propyl nitrite recorded with a resolution of 1 cm^{-1} . (a) Matrix deposition with effusion source ($p \approx 1\text{ bar}$), 10 K . (b) Matrix deposition with pulsed supersonic jet inlet ($\nu_{\text{imp}} = 4\text{ Hz}$, $p \approx 1\text{ bar}$, 1:2000 dilution). (c) Matrix deposition with pulsed supersonic jet inlet ($\nu_{\text{imp}} = 6\text{--}9\text{ Hz}$, $p \approx 1\text{ bar}$, 1:2000 dilution).

reasons. First, the peaks of the five syn conformers overlap much more than the peaks of the three anti conformers. Second, the relative abundance of the syn conformers is lower. Third, they decompose faster during the UV–vis irradiation than the anti forms.

The rates of change in the intensity of the anti conformer peaks upon irradiation showed a moderate variation between peaks. The most pronounced differences were observed for the peaks around 800 and 1650 cm^{-1} . Utilizing this observation, we can collect peaks of the groups of anti conformers with similar decomposition rates. Sorting these to individual conformers is possible only by the help of supersonic jet-matrix experiments and theoretical calculations.

When the results of jet-matrix experiments are analyzed, it is conspicuous that the relative intensities of the syn and anti bands, where the unresolved peaks of the individual conformers accidentally overlap, are nearly unaltered when the measurement is switched from the effusive inlet source to supersonic jet deposition. On the other hand, the relative intensity of the individual peaks belonging to either the syn group or the anti is notably different under effusive and jet deposition conditions (see spectra a and b or a and c in Figure 5). Furthermore, the intensity of some peaks changed slightly even with a minor change of experimental conditions (see spectra b and c in Figure 5).

A coherent explanation of this complex picture can be given using the results of quantum chemical calculations for conformer abundances and energy barriers. Calculations showed that energy barriers along the path of syn–anti interconversion are high, above 50 kJ/mol ; hence conformational cooling cannot be expected under our supersonic expansion conditions. This is exactly in line with our observations. On the other hand, as discussed before, interconversion among different syn or different anti conformers is expected during supersonic expansion, because the corresponding energy barriers are predicted to be smaller than 20 kJ/mol . This is again compatible with the experimental findings. Finally, barriers along the ϕ_2 NOCC torsion are low, which explains that the intensity of some peaks, and hence the abundances of some conformers, can depend even on the matrix deposition conditions.

Assignment of the anti conformers in the spectra can be started from the group of peaks around 800 cm^{-1} . The intensity of the peak at 796 cm^{-1} slightly decreased in the matrix deposited with supersonic expansion, but it was not strongly

TABLE 6: Abridged Assignment of the MI-IR Spectrum of *n*-Propyl Nitrite

$\tilde{\nu}_{\text{obs}}$	I_{obs}^a	Ph ^b	jet ^c	theo ^d	$\tilde{\nu}_{\text{calc}}^d$	I_{calc}^d	TED ^e
1661	vs	anti	A+St-G-	A+St-G-	1701	235	94% stre O1N2
1659	vs	anti	ASt-G+	ASt-G+	1701	230	94% stre O1N2
1656	vs	anti	A+St-T-	A+St-T-	1700	242	94% stre O1N2
1607	s	syn		STT; ST+G-;	1629; 1630;	163; 147;	95% stre O1N2
				SG-T-; SG-G-;	1637; 1638;	147; 149;	94% stre O1N2
1605	s	syn		SSt-G+	1648	159	94% stre O1N2
1050	m	anti	A+St-T-	A+St-T-	1035	31	55% stre O3C4, 14% stre C4C5, 20% bend O3N2O1
988	m	syn	SG-T-	SG-T-	977	137	37% stre O3C4, 34% bend O3N2O1
984	m	syn	STT	STT	983	111	36% stre O3C4, 34% bend O3N2O1
963	m	syn	ST+G-	ST+G-	966	143	21% stre O3C4, 39% bend O3N2O1
961	m	syn	SSt-G+/SG-G-	SG-G-	968	122	19% stre O3C4, 37% bend O3N2O1
951	w		SSt-G+/SG-G-	SSt-G+	954	120	20% stre O3C4, 40% bend O3N2O1
918	m	anti	ASt-G+	ASt-G+	917	69	15% bend H12C6C5, 18% bend H13C6C5
833	m	syn	STT/ST+G-	ST+G-	840	92	24% stre N2O3, 11% stre C5C6, 14% bend O3N2O1
831	m	syn	SSt-G+/SG-G-	SG-G-	829	13	13% stre O3C4, 13% stre C4C5, 17% stre C5C6
805	vs	anti	ASt-G+	ASt-G+	820	287	22% stre N2O3, 19% stre O3C4, 20% bend O3N2O1
796	vs	A+St-T-	A+St-T-	A+St-T-	821	296	23% stre N2O3, 18% stre O3C4, 27% bend O3N2O1
789	s	A+St-G-	A+St-G-	A+St-G-	802	288	24% stre N2O3, 17% stre O3C4, 21% bend O3N2O1
770	m	A+St-G-	A+St-G-	A+St-G-	770	17	14% bend H12C6C5
762	m	ASt-G+	ASt-G+	ASt-G+	764	67	15% stre N2O3, 12% bend H11C6C5
704	w	syn	ST+G-	ST+G-	723	126	48% stre N2O3
639	m	A+St-T-		A+St-T-	632	80	56% stre N2O3, 16% bend O3N2O1
597	w	ASt-G+		ASt-G+	597	38	39% stre N2O3, 22% bend O3N2O1, 10% bend C5C4O3

^a $\tilde{\nu}_{\text{obs}}$: measured frequency in cm^{-1} ; I_{obs} : measured intensity (w, weak; m, medium; s, strong; vs, very strong). ^b Ph.: assignment by the different photodecomposition rates. ^c Jet: assignment by conformational cooling with supersonic jet deposition. ^d Obtained at the SQM B3LYP/6-31G* level of theory ($\tilde{\nu}_{\text{calc}}$ in cm^{-1} , I_{calc} in km/mol units). ^e TED: total energy distribution of normal modes (components with a ratio higher than 10%) over internal coordinates (stre, stretching; bend, bending; tors, torsional coordinate). Labels are in agreement with Figure 2.

affected by the experimental conditions (see spectra b and c in Figure 5). Theoretical calculations showed that among the three anti conformers A+St-G- and ASt-G+ are connected by low-lying barriers; hence the peak at 796 cm^{-1} was assigned to the third, A+St-T- conformer. Other peaks with a similar behavior were found at 1066, 1050, 639, and 617 cm^{-1} . The rates of decrease upon UV-vis irradiation were found to be similar for most of these peaks as well. It can thus be concluded that among the anti conformers the A+St-T- conformer decomposed the most slowly upon UV-vis irradiation.

To continue the analysis, we consider the peak at 805 cm^{-1} . This peak gained intensity under supersonic jet deposition conditions as compared to the case for effusive deposition, but its actual relative intensity also depended on the experimental conditions. Its intensity variation was inversely "correlated" with the intensity of the peak centered at 789 cm^{-1} . In spectrum c of Figure 5 the relative intensity of the peak at 789 cm^{-1} increased compared to that in spectrum b, when the matrix was deposited more slowly, and the intensity of the peak at 805 cm^{-1} decreased slightly. From these results the peak at 805 cm^{-1} was assigned to ASt-G+ and the one at 789 cm^{-1} to A+St-G-. Of the most intense peaks that showed a similar dependence, the ones at 904, 882, 789, 770, and 580 cm^{-1} were assigned to the A+St-G- conformer, and the peaks at 1071, 1052, 918, 805, 762, 758, and 597 cm^{-1} to ASt-G+. Comparing these results with photodecomposition rates, one can conclude that under the present experimental conditions A+St-G- decomposed the most rapidly, and the rate of decomposition of the ASt-G+ form was slower.

As to the syn conformers, due to the shallow interconversion paths between these conformers, characteristic intensity changes were observed for several peaks. The most prominent three groups of peaks around 984, 963 and 833 cm^{-1} , assigned to syn conformers on the basis of the photochemical experiments, were considered. The intensity of the peak at 963 cm^{-1} clearly increased under supersonic jet conditions, but on the basis of the intensity dependencies, the peak at 961 cm^{-1} certainly belongs to a conformer that is connected with the former one

via a low-energy barrier and has higher energy. Thus, the peak at 963 cm^{-1} was assigned to the thermodynamically most stable syn conformer, ST+G-. The peak at 961 cm^{-1} can be assigned to either the SG-G- or the SSt-G+ conformers, which are connected to ST+G- via a barrier less than 5 kJ/mol. The relative intensity of the peak at 984 cm^{-1} also increased under supersonic expansion conditions and its intensity was only slightly dependent upon experimental conditions. On the other hand, the peak in its neighborhood at 988 cm^{-1} was decreased in jet deposition and it was again only slightly affected by changes in the experimental conditions. On the basis of these findings and the calculated barrier heights and relative energies, the peak at 984 cm^{-1} was assigned to STT, and the peak at 988 cm^{-1} to SG-T-. As a result of this complex analysis all the eight predicted conformers were identified in the spectra and the observed vibrational transitions were assigned to the calculated normal modes of individual conformers. See Table 6 or the Supporting Information for further details.

4.2.2. Products of UV-Vis Photolysis. 4.2.2.a. Isopropyl Nitrite. On the basis of the peaks appearing at 3010 and 1568 cm^{-1} , one of the main products of UV-visible photolysis of isopropyl nitrite isolated in argon matrix is nitroxyl, HNO. This is in good agreement with photolysis studies on other primary and secondary alkyl nitrites.^{18,19,22,24} If the reaction path is the same as was supposed for these former studies, then HNO can be produced when NO, one of the primary photoproducts, subtracts a hydrogen atom from the isopropoxy radical, the other primary product, resulting in the other secondary product, acetone. This assumption can be confirmed by the peaks observed at 3017, 2974, 2935, 1720, 1444, 1432, 1365, 1217, 1092, and 533 cm^{-1} , which can unambiguously be assigned to acetone on the basis of literature data.³⁸ Earlier studies also reported the formation of the 1:1 complex of an aldehyde or ketone and HNO. In the present case the peaks observed at 1712, 1574, 1514, and 1513 cm^{-1} reveal the formation of the acetone HNO complex.

The former studies²³ suggest that NO can break not only the C-H bond but also the C-C bond. In agreement with this,

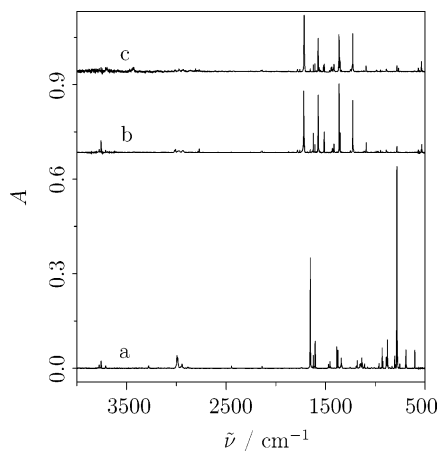


Figure 6. Infrared spectra measured with a resolution 0.5 cm^{-1} before and after a prolonged photolysis of isopropyl nitrite. (a) Isopropyl nitrite in argon matrix. (b) Spectrum after 4 h of broadband UV–vis irradiation. (c) Spectrum recorded at 8 K after 4 h of photolysis followed by annealing at 35 K.

prolonged irradiation resulted in the production of nitrosomethane, which had been identified by the peaks appearing at 1553, 1416, and 1349 cm^{-1} .²³ The other product, acetaldehyde, was appearing at 2735, 1739, 1729, 1436, 1427, 1351, 1120, 1116, and 509 cm^{-1} in the infrared spectra as expected.³⁹ In this general reaction scheme an alkoxy radical is formed in the first step, although, as it was mentioned before, it was identified in the matrix only by one study using laser-induced fluorescence detection.²⁵ In the present experiments a small amount of nitrogen monoxide (appearing at 1873 cm^{-1} as in ref 40) was observed after the UV–vis irradiation of isopropyl nitrite. The molar absorption coefficients of the isopropoxy radical, which is supposed to be produced as the other product of the first step, are expected to be smaller than that of NO. Consequently, extremely weak peaks should belong to the isopropoxy radical in our spectrum. Because the isopropoxy radical is a reactive species, it can exist on a longer time scale in the low-temperature Ar matrix, but it should react with small diffusing molecules, e.g., nitrogen monoxide, nitroxyl, or water traces at 20–30 K. Thus the peaks of isopropoxy radical should disappear from the spectrum when the matrix is annealed.

After the annealing of the photolyzed matrix sample, slight changes were observed in the spectrum (see the spectra b and c in Figure 6). As an example, the peaks of acetone decreased due to the diffusion of traces of water, and at 1716, 1419, 1367, 1358, 1231, 1094, and 537 cm^{-1} new peaks, corresponding to the acetone–water complex,³⁸ appeared. Appearing/increasing peaks at 2806, 1564, and 1506 cm^{-1} reveal the complexation of HNO most likely with acetone or acetaldehyde. As a conclusion, most of the spectral changes caused by annealing and hence due to the diffusion of small molecules can be explained by the formation of hydrogen-bonded complexes.

However, there are four tiny peaks in the $1200\text{--}900\text{ cm}^{-1}$ region, at 1108, 980, 975, and 971 cm^{-1} , which completely disappeared during the annealing process (see Figure 7) and cannot be assigned to any of the above-mentioned species. Several possibilities can be considered for their origin. First, they might originate from an unfavorable orientation of species in the argon lattice that had relaxed during the annealing. Second, they can correspond to an uncomplexed species that forms a complex with small, diffusing molecules. Third, the presence and reactions of isopropoxy radical cannot be excluded, because in the supersonic jet-disperse fluorescence measurements⁴¹ some of their transitions were found in this region.

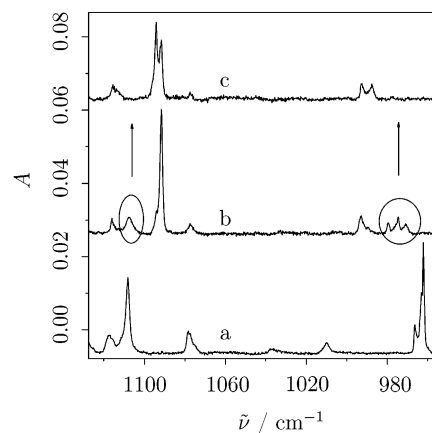


Figure 7. Infrared spectra measured with a resolution 0.5 cm^{-1} before and after a prolonged photolysis of isopropyl nitrite. Enlargement of the $960\text{--}1120\text{ cm}^{-1}$ spectral region. (a) Isopropyl nitrite in argon matrix at 8 K. (b) Spectrum after 4 h of broadband UV–vis irradiation, 8 K. (c) Spectrum recorded at 8 K after 4 h of photolysis followed by annealing at 35 K.

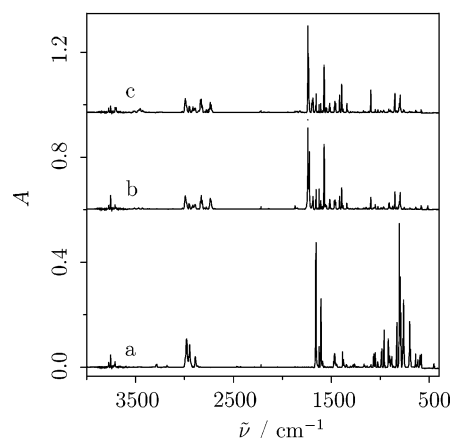


Figure 8. Infrared spectra measured with a resolution 1 cm^{-1} before and after a prolonged photolysis of *n*-propyl nitrite. (a) *n*-Propyl nitrite in argon matrix. (b) Spectrum after 70 min of broadband UV–vis irradiation, 10 K. (c) Spectrum recorded at 10 K after 70 min of photolysis followed by annealing at 34 K.

For a detailed analysis of the photolysis products and the processes identified upon annealing the matrix, see the Supporting Information.

4.2.2.b. *n*-Propyl Nitrite. As expected from the general decomposition paths of alkyl nitrites, one of the main products of broadband UV–vis irradiation of matrix isolated *n*-propyl nitrite yielded nitroxyl and its complexed forms, which can be identified on the basis of the peaks appearing at 1575, 1573, 1521, 1519, 1516, and 1511 cm^{-1} .^{18,19,22,24} The other main product is propanal, which is formed both in the lower-energy trans form, appearing at 2982, 2948, 2906, 2900, 2890, 2726, 1741, 1736, 1733, 1693, 1468, 1462, 1416, 1394, 1343, 1340, 1099, 1095, 855, and 852 cm^{-1} , and in the higher-energy gauche form, as expected^{42,43} to appear at 1726, 1144, 1142, 1115, 1112, 912, 910, 875, 871, 869, and 515 cm^{-1} in the IR spectrum. (Note that, unlike refs 42 and 43, here we labeled the conformation around the OCCO torsion by the gauche and trans notations.)

The bands observed at 3453, 1557, and 1172 cm^{-1} (Figure 8) most probably belong to *cis*-1-nitrosopropanol, because the transitions of its homologues, e.g., nitrosomethanol and nitrosoethanol, were found at similar positions, {3478, 1559, and

1131} and {3459, 1552, and 1176} cm^{-1} , respectively.^{20,21,22} Vibrational transition of one of the primary reaction products, NO, was also observed with low intensity at 1872 cm^{-1} .

The most important process observed upon annealing the matrix is the *gauche* \rightarrow *trans* relaxation of propanal. In this case none of the disappearing peaks or peaks with decreasing intensities could be attributed to the reactive *n*-propoxy radical, the primary product of the photodecomposition.

For further details of the assignments, see the Supporting Information.

5. Summary

In the present study the conformational landscape and the photochemical properties of isopropyl nitrite and *n*-propyl nitrite were investigated.

Conformational analysis was carried out with the help of three complementary methods. First, theoretical calculations, performed at the G2 and SQM-B3LYP/6-31G* levels of theory, predicted conformer distributions and vibrational frequencies of the different conformers. On the basis of these calculations three isopropyl nitrite and eight *n*-propyl nitrite conformers are expected to be present in thermodynamic equilibrium in the vapor phase at room temperature.

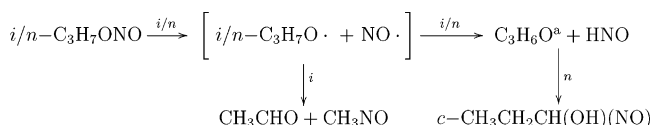
The second, experimental method utilized the fact that the different conformers of propyl nitrites decompose with different rates upon UV-vis irradiation of the matrix and their decomposition products recombine with different rates. With the help of quantum chemical calculations, first the anti and syn conformers were identified in the spectra. After this, it was proven that, in agreement with chemical intuition, the rate of photodecomposition depends mainly on the steric alignment of the ONOC torsion, i.e., anti and syn.

Finally, in the case of *n*-propyl nitrite, conformational cooling was achieved with supersonic jet deposition, which also helped the identification of conformers. To understand the cooling effect, barrier heights between the conformers were calculated at the B3LYP/6-31G* level of theory. These calculations showed that conformational cooling along the ONOC torsion cannot be expected, because the barriers along this coordinate are high, on the order of 50 kJ/mol. The barrier heights are much lower along the OCCO and NOCC torsional coordinates, on the order of 10–20 and \sim 5 kJ/mol, respectively. In line with expectations, it was found that jet cooling is efficient along both of these coordinates. Furthermore, due to the very low barriers along the NOCC torsion, not only were conformational changes achieved by supersonic expansion but also the conformer ratio in the matrix varied upon the deposition conditions, because the energy release of the impacting molecular beam is high enough to overcome these barriers. This fact has not only complicated the spectra but also yielded distinct information on the conformers that interconvert to each other along the OCCO and NOCC torsional coordinates.

As a result of the conformational analysis, two to three conformers of isopropyl nitrite and eight conformers of *n*-propyl nitrite were identified and assigned in the matrix-isolation infrared spectra.

When matrix-isolated isopropyl nitrite was photolyzed by UV-vis light, acetone and nitroxyl and their 1:1 complex were mainly formed. Besides these products, acetaldehyde and nitrosomethane were produced along a different reaction path. Furthermore, small amounts of the primary photolysis product, NO, was observed, as well. The presence of its counterpart product, isopropoxy radical cannot unambiguously be proved by the analysis of infrared spectra. The main signs that reveal

SCHEME 1: Photochemical Reaction Scheme of Propyl Nitrites in Argon Matrix^a



^a C₃H₆O: propanone/propanal.

its existence in the matrix are the low-intensity peaks in the 1200–900 cm^{-1} region. These features disappeared upon annealing the matrix, which could not be explained by any viable complexation or relaxation process.

In the case of UV-vis photolysis of *n*-propyl nitrite, *trans*- and *gauche*-propanal, nitroxyl, and their 1:1 complex were formed. In a small amount another product, most likely *cis*-1-nitrosopropanol, was also produced. Furthermore, infrared transition of one of the primary reaction products, NO, was also observable in the spectra, but no evidence was found for the presence of *n*-propoxy radical, the other primary product. The most dominant changes in the infrared spectra upon annealing the matrix corresponded to the *gauche* \rightarrow *trans* relaxation of propanal. A general overview of observed reaction paths is given in Scheme 1.

As a future project the wavelength dependence of the photolysis processes could be investigated. Such a study could unambiguously explain our present observations that the syn conformers of isopropyl nitrite decompose faster, whereas using the same broadband UV-vis irradiation source, the anti conformers of *n*-propyl nitrite decompose more rapidly. Wavelength-dependent photolysis studies could also yield more information on the different decomposition paths of propyl nitrites.

Acknowledgment. This work has been funded by the Hungarian Ministry of Education (FKFP 0131/2001 and GVOP-3.2.1-2004-04-0010/3.0) and the Hungarian Scientific Research Fund (OTKA F049722 and T047186). G.T. also acknowledges the support of the Zoltán Magyar Foundation.

Supporting Information Available: Optimized geometries at the B3LYP/6-31G* level of theory, SQM-B3LYP/6-31G* infrared frequencies and intensities of each conformer, detailed assignments of infrared spectra of matrix isolated isopropyl and *n*-propyl nitrites and that of the photolyzed samples in matrices, as well as the full author list of ref 33. This material is available free of charge via the Internet at <http://pubs.acs.org>.

References and Notes

- Orlando, J. J.; Tyndall, G. S.; Wallington, T. J. *Chem. Rev.* **2003**, *103*, 4657.
- Vidya, V.; Sankaran, K.; Viswanathan, K. S. *Chem. Phys. Lett.* **1996**, *258*, 113.
- Kudoh, S.; Takayanagi, M.; Nakata, M. *Chem. Phys. Lett.* **1998**, *296*, 329.
- Felder, P.; Günthard, H. H. *Chem. Phys. Lett.* **1979**, *66*, 283.
- Felder, P.; Günthard, H. H. *Chem. Phys.* **1982**, *60*, 9.
- Vidya, V.; Sankaran, K.; Sundarajan, K.; Viswanathan, K. S. *J. Mol. Struct.* **1999**, *476*, 97.
- Venkatesan, V.; Sundarajan, K.; Viswanathan, K. S. *Spectrochim. Acta A* **2002**, *58*, 467.
- Venkatesan, V.; Sundarajan, K.; Viswanathan, K. S. *J. Phys. Chem. A* **2002**, *106*, 7707.
- Ito, F.; Nakanga, T.; Futami, Y.; Kudoh, S.; Takayanagi, M.; Nakata, M. *Chem. Phys. Lett.* **2001**, *343*, 185.
- Futami, Y.; Kudoh, S.; Takayanagi, M.; Nakata, M. *Chem. Phys. Lett.* **2002**, *357*, 209.
- Futami, Y.; Kudoh, S.; Ito, F.; Nakanaga, T.; Nakata, T. *J. Mol. Struct.* **2004**, *690*, 9.

- (12) Kodoh, S.; Onoda, K.; Takayanagi, M.; Nakata, M. *J. Mol. Struct.* **2000**, *524*, 61.
- (13) Sankaran, K.; Vidya, V.; Viswanathan, K. S.; George, L.; Singh, S. *J. Phys. Chem. A* **1998**, *102*, 2944.
- (14) Levy, D. H. *Science* **1981**, *214*, 4518.
- (15) Godfrey, P. D.; Brown, R. D.; Rodgers, F. M. *J. Mol. Struct.* **1996**, *376*, 65 and citations therein.
- (16) Brown, H. W.; Pimentel, G. C. *J. Chem. Phys.* **1958**, *29*, 883.
- (17) Jacox, M. E. *J. Phys. Chem.* **1984**, *88*, 3373.
- (18) Jacox, M. E.; Rock, F. L. *J. Phys. Chem.* **1982**, *86*, 2899.
- (19) Müller, R. P.; Russegger, P.; Huber, J. R. *Chem. Phys.* **1982**, *70*, 281.
- (20) Müller, R. P.; Huber, J. R. *J. Phys. Chem.* **1983**, *87*, 2460.
- (21) Müller, R. P.; Huber, J. R.; Hollenstein, H. *J. Mol. Spectrosc.* **1984**, *104*, 209.
- (22) Müller, R. P.; Nonella, M.; Huber, J. R. *Helv. Chim. Acta* **1984**, *67*, 953.
- (23) Barnes, A. J.; Hallam, H. E.; Waring, S.; Armstrong, J. R. *J. Chem. Soc., Faraday Trans. 2* **1976**, *67*, 1.
- (24) Puchowicz, D.; Adamus, J.; Ćebicki, J. *J. Chem. Soc., Perkin Trans. 2* **2000**, 1942.
- (25) Chiang, S.-Y.; Hsu, Y.-C.; Lee Y.-P. *J. Chem. Phys.* **1989**, *90*, 81.
- (26) Engert, J. M.; Dick, B. *Chem. Phys. Lett.* **1999**, *299*, 423.
- (27) Felder, P.; Ha, T.-K.; Dwivedi A. M.; Günthard, Hs. H. *Spectrochim. Acta* **1981**, *37 A*, 337.
- (28) Turner, P. H. *J. Chem. Soc., Faraday Trans.* **1979**, *2*, 317.
- (29) In *Organic Synthesis*; Blatt, A. H., Ed.; Wiley: New York, 1948; Collect. Vol. II, pp 108–109.
- (30) Becke, A. D. *J. Chem. Phys.* **1993**, *98*, 5648.
- (31) Lee, C.; Yang, W.; Parr, R. G. *Phys. Rev. B* **1998**, *37*, 785.
- (32) Curtiss, L. A.; Raghavachari, K.; Trucks, G. W.; Pople, J. A. *J. Chem. Phys.* **1991**, *94*, 7221.
- (33) Frisch, M. J.; et al. *Gaussian 03*, revision B.05.
- (34) Pulay, P.; Fogarasi, G.; Pongor, G.; Boggs, J. E.; Vargha, A. *J. Am. Chem. Soc.* **1983**, *105*, 7037.
- (35) Baker, J.; Jarzecki, A. A.; Pulay, P. *J. Phys. Chem. A* **1998**, *102*, 1412.
- (36) Pulay, P.; Török, F. *Acta Chim. Sci. Hung.* **1965**, *47*, 273.
- (37) PQS version 3.2, Parallel Quantum Solutions, 2013 Green Acres Rd., Fayetteville, AR 72703.
- (38) Zhang, X. K.; Lewars, E. G.; March, R. E.; Parnis, J. M. *J. Phys. Chem.* **1993**, *97*, 4320.
- (39) Hawkins, M.; Andrews, L. *J. Am. Chem. Soc.* **1983**, *105*, 2523.
- (40) Saxce, A. de; Sanna, N.; Schriver, A.; Schriver-Mazzuoli, L. *Chem. Phys.* **1994**, *185*, 365.
- (41) Jin, J.; Sioutis, I.; Tarczay, G.; Gopalakrishnan, S.; Bézant, A.; Miller, T. A. *J. Chem. Phys.* **2004**, *121*, 11780.
- (42) Gupta, V. P.; Lotta, T.; Murto, J.; Räsänen, M.; Aspiala, A. *Chem. Phys.* **1984**, *90*, 291.
- (43) Frankiss, S. G.; Kynaston, W. *Spectrochim. Acta* **1972**, *28 A*, 2149.